Bypassing a 8,5′-cyclo-2′-deoxyadenosine lesion by human DNA polymerase η at atomic resolution

Peter J. Weng[a,1,2], Yang Gao[a,1], Mark T. Gregory[a,1,3], Pengcheng Wang[b], Yinsheng Wang[b,4], and Wei Yang[a,4]

[a]Laboratory of Molecular Biology, National Institute of Diabetes and Digestive and Kidney Diseases, National Institutes of Health, Bethesda, MD 20892; and [b]Department of Chemistry, University of California, Riverside, CA 92521-0403

Contributed by Wei Yang, August 28, 2018 (sent for review July 25, 2018; reviewed by Philip John Brooks and Hong Ling)

Oxidatively induced DNA lesions 8,5′-cyclopurine-2′-deoxynucleosides (cdPus) are prevalent and cytotoxic by impeding DNA replication and transcription. Both the 5′*R*- and 5′*S*-diastereomers of cdPu can be removed by nucleotide excision repair; however, the 5′*S*-cdPu is more resistant to repair than the 5′*R* counterpart. Here, we report the crystal structures of human polymerase (Pol) η bypassing 5′*S*-8,5′-cyclo-2′-deoxyadenosine (cdA) in insertion and the following two extension steps. The cdA-containing DNA structures vary in response to the protein environment. Supported by the "molecular splint" of Pol η, the structure of 5′*S*-cdA at 1.75-Å resolution reveals that the backbone is pinched toward the minor groove and the adenine base is tilted. In the templating position, the cdA takes up the extra space usually reserved for the thymine dimer, and dTTP is efficiently incorporated by Pol η in the presence of Mn^{2+}. Rigid distortions of the DNA duplex by cdA, however, prevent normal base pairing and hinder immediate primer extension by Pol η. Our results provide structural insights into the strong replication blockage effect and the mutagenic property of the cdPu lesions in cells.

context-dependent | DNA distortion | Mg^{2+} | Mn^{2+} | Ca^{2+}

Reactive oxygen species and the resulting DNA lesions occur routinely in all life. In addition to the most common oxidative lesion 8-oxo-7,8-dihydro-2′-deoxyguanosine (8-oxo-dG), 8,5′-cyclo-2′-deoxyadenosine (cdA) and 8,5′-cyclo-2′-deoxyguanosine (cdG) are frequently induced in DNA by hydroxyl radicals produced from Fenton-type reactions or ionizing radiation (1). Different from simple nucleobase modifications, such as 8-oxo-dG, which is efficiently cleaved and removed by glycosylase and base-excision repair (2), the cyclization between the base (C8) and sugar backbone (C5′) via C4′-O4′-C1′-N9 cannot be resolved by glycosylase and has to be removed as a stretch of nucleotides by nucleotide excision repair (NER) (3–6). The NER pathway is required primarily to remove DNA lesions caused by UV irradiation (7). Therefore, NER deficiencies lead not only to UV sensitivity and a condition known as xeroderma pigmentosum, but also to accumulation of cdA and cdG and neurodegenerative diseases (1, 8, 9). Unrepaired 8,5′-cyclopurines obstruct normal DNA replication and transcription (10, 11) and induce mutagenesis. Specialized translesion DNA polymerases (Pols) can partially bypass cdPu lesions (10, 12). Sensitive methods of detecting cellular cdPu (8, 13) have revealed that the 5′*R* and 5′*S* diastereomers of cdPu exist in normal tissues, and the *S*-cdA is prevalent as a result of its resistance to NER removal (1, 6). Furthermore, the amount of cdA and cdG accumulates with aging in WT mice and is suspected to contribute to progressive neurodegeneration (8, 14).

Since the discovery of 8,5′-cyclopurines in DNA three decades ago, solution structures of DNA containing a 5′*S*-cdG have been determined by NMR (15, 16). Interestingly, in the NMR structures, distortion of the backbone from the normal B-form DNA is mild, and the duplex remains fully base-paired. Investigation of the impediment and mutagenic roles of 5′*S*-cdA in transcription by X-ray diffraction of yeast RNA Pol II reveals that the lesion fails to occupy the active site, as does a normal dA, and behaves somewhat like UV-induced thymine dimer (11). Because of the cdA being at single- and double-strand junctions in the cocrystal structures of RNA Pol and the resolution limits of 4 Å (11), how an 8,5′-cyclopurine deforms a DNA double helix, thus inhibiting replication and transcription, remains unclear. In 2015, the crystal structures of archaeal Y-family DNA Pol Dpo4 complexed with 5′ S-cdG was reported (17). Although Dpo4 bypasses 5′*S*-cdG in a template-dependent manner in solution (17), in the crystal structures, cdG does not form a base pair with an incoming dCTP or dTTP because it is displaced into the major groove or flips out of the active site entirely. How DNA Pol carries out translesion synthesis opposite and past 8,5′-cdPu is still unknown.

To find out structural distortions of DNA by cdPu and how DNA Pol η, specialized in TLS of UV lesions, helps in bypassing the lesions, we focus our studies on 5′*S*-cdA (Fig. 1*A*), which is present at appreciable levels in animal tissues (8, 13). Nucleotide incorporation analyses show that *S*-cdA is accommodated in the active site of DNA Pol η and can direct the incorporation of dTTP. Pol η also has limited ability to extend DNA primers after

Significance

This series of structural analysis of human DNA polymerase (Pol) η bypassing 5′*S*-8,5′-cyclo-2′-deoxyadenosine (cdA) reveals context-dependent DNA distortions caused by this oxidative damage. DNA Pol η is most efficient in nucleotide incorporation opposite a cdA and least efficient in extending the primer immediately following cdA. This study also graphically illustrates the difference between Mg^{2+}, Mn^{2+}, and Ca^{2+} and their varied capabilities in recruiting and orienting dNTP in the DNA Pol active site when the templating base is damaged. The physiologically abundant Mg^{2+} is extremely sensitive to its coordination environment and fails to support base pairing, let alone the productive substrate alignment. Mn^{2+}, however, allows proper dNTP binding and incorporation even with a damaged template. Ca^{2+} may permit base pairing, but the substrate alignment is incompatible with catalysis.

Author contributions: W.Y. designed research; P.J.W., Y.G., and M.T.G. performed research; P.W. and Y.W. contributed new reagents/analytic tools; P.J.W., Y.G., M.T.G., Y.W., and W.Y. analyzed data; and P.J.W., Y.G., M.T.G., Y.W., and W.Y. wrote the paper.

Reviewers: P.J.B., NIH; and H.L., University of Western Ontario.

The authors declare no conflict of interest.

Data deposition: The atomic coordinates and structure factors reported in this paper have been deposited in the Protein Data Bank, https://www.wwpdb.org/ (PDB ID codes 6M7O, 6M7P, 6M7T, 6M7U, and 6M7V).

[1]P.J.W., Y.G., and M.T.G. contributed equally to this work.

[2]Present address: Scientist Training Program, Duke University School of Medicine, Durham, NC 27710.

[3]Present address: NanoString Technologies, Seattle, WA 98109.

[4]To whom correspondence may be addressed. Email: yinsheng.wang@ucr.edu or wei.yang@nih.gov.

This article contains supporting information online at www.pnas.org/lookup/suppl/doi:10.1073/pnas.1812856115/-/DCSupplemental.

Published online October 1, 2018.

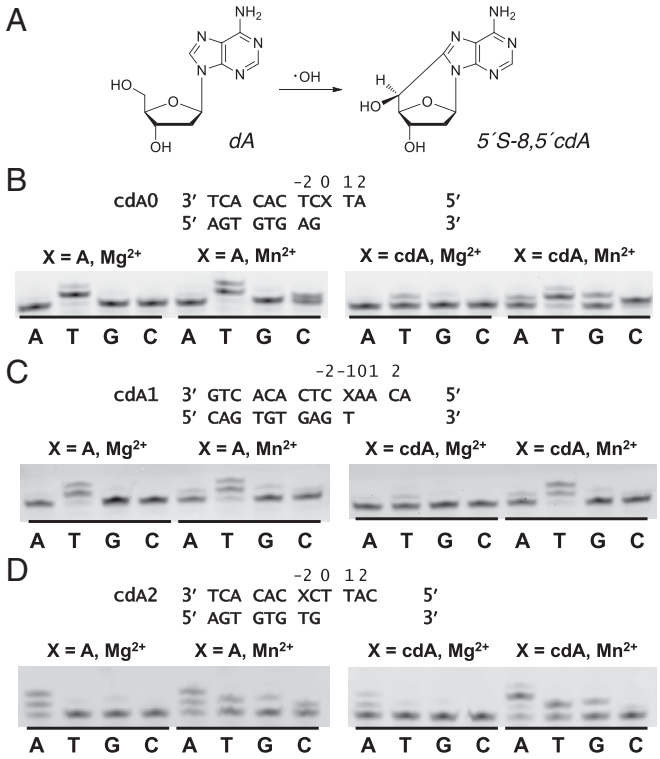

Fig. 1. Bypass of 5′*S*-cdA by human Pol η. (*A*) Formation of *S*-cdA from a normal dA by oxidation. (*B*) Comparison of dNTP selection and incorporation efficiency when dA or cdA is the templating nucleotide. The assays were performed in the presence of Mg^{2+} or Mn^{2+} and 100 μM of each dNTP (G, A, T, or C). The DNA oligos used are shown above the gels. (*C* and *D*) Primer extension with dA or cdA (X) at −1 (*C*) or −2 (*D*) position upstream from the 3′ end of the primer.

cdA, but the efficiency and accuracy are both reduced significantly. By using X-ray crystallography, we have examined the nucleotide insertion opposite *S*-cdA and primer extension afterward and obtained five representative structures. The structure of primer extension with cdA lesion embedded in the DNA duplex, which was determined at 1.75-Å resolution, reveals why the lesion may resist NER yet causes strong blockage to DNA and RNA Pols. Structural analyses of the nucleotide insertion opposite cdA in the presence of Mg^{2+}, Ca^{2+}, and Mn^{2+} also reveal that Mg^{2+} is the most sensitive to the coordination environment and least tolerant of distorted DNA. Meanwhile, Mn^{2+} relaxes nucleotide selection by DNA Pol and makes Pol η "blind" to the lesion-distorted DNA at the cost of increased misincorporation.

Results

TLS of *S*-cdA by Human Pol η. The Y-family DNA Pol η, which is specialized in bypassing UV-induced thymine dimers, has been reported to bypass *S*-cdA lesions efficiently (10, 18). With the ultrapure and active human DNA Pol η core protein (residues 1–432), we first checked the nucleotide choice and efficiency in the insertion and extension steps of bypassing *S*-cdA (Fig. 1). In the insertion step, Pol η prefers to incorporate dTTP opposite *S*-cdA similar to when a normal dA is the templating nucleoside. dGTP is also incorporated at a lower efficiency (Fig. 1*B* and Table 1). In the presence of Mg^{2+}, k_{cat} of bypass incorporation is reduced to less than 10% compared with a normal dA, but the large reduction in the efficiency of dTTP incorporation is a result of the >100× increase in K_M. Replacement of Mg^{2+} with Mn^{2+}, however, fully rescues the dTTP binding opposite cdA and restores the bypass efficiency in the insertion step to almost normal. Depending on DNA sequences, Mn^{2+} also improves the DNA synthesis efficiencies of Pol η with undamaged templates by 1.3–9.3 fold (Table 1).

It has been established that translesion synthesis often requires two different specialized Pols to carry out the insertion and extension steps, respectively (19, 20). This is because differently damaged bases need different active sites to accommodate them in the insertion step (21). When lesions are beyond the active site in the primer extension step, they all distort and destabilize the DNA double-helix structure and thus interfere with normal interactions with DNA Pols. One common feature of lesion-containing DNAs is the reduced duplex rigidity (22), and therefore different lesions embedded in a duplex may be accommodated by a similar looping-out mechanism for primer extension (23, 24).

As shown previously, human DNA Pol η has low activity in extending primers after cdA (10). In the presence of Mg^{2+}, the efficiencies of primer extension immediately after *S*-cdA was reduced by nearly 1 million fold compared with the efficiencies with normal DNA (Fig. 1*C* and Table 1). Interestingly, in the presence of Mn^{2+}, Pol η recovered ∼10% primer-extension efficiency by a dramatically reduced K_M and increased binding affinity for an incoming nucleotide. Bypass of *S*-cdA in vivo likely depends on Pol ζ, which is specialized in extension step of TLS (12). In contrast, when *S*-cdA was 1 bp further away from the active site (2 bp upstream), the Mg^{2+}-dependent primer extension by Pol η was only slightly less efficient than dTTP incorporation opposite the lesion (Fig. 1*D* and Table 1).

Structure and DNA Distortions of *S*-cdA. Cocrystallizing Pol η and DNA containing a cdA lesion was rather difficult. One possible reason was disruption of the active site as evidenced by the low Pol activity of Pol η in the presence of Mg^{2+} and low efficiency in primer extension even in the presence of Mn^{2+}. With perseverance,

Table 1. Kinetic parameters of dNTP incorporation by Pol η

DNA	dNTP	Me^{2+}	K_M, μM	k_{cat}, min^{-1}	k_{cat}/K_M, $min^{-1}.\mu M^{-1}$	Relative efficiency
CdA0, X = A	dT	Mg^{2+}	5.4 (0.7)	109 (13)	20	1
CdA0, X = cdA	dT	Mg^{2+}	570 (70)	8.6 (0.5)	0.015	6.7×10^{-4}
CdA0, X = A	dT	Mn^{2+}	0.44 (0.04)	82 (5)	186	1
CdA0, X = cdA	dT	Mn^{2+}	0.49 (0.07)	10.1 (0.2)	21	0.11
CdA1, X = A	dT	Mg^{2+}	4.3 (0.3)	80 (2)	19	1
CdA1, X = cdA	dT	Mg^{2+}	1,030 (210)	0.07 (0.01)	6.7×10^{-5}	3.4×10^{-6}
CdA1, X = A	dT	Mn^{2+}	0.76 (0.16)	19.4 (0.8)	25.5	1
CdA1, X = cdA	dT	Mn^{2+}	0.51 (0.05)	1.2 (0.1)	2.4	9.4×10^{-2}
CdA2, X = A	dA	Mg^{2+}	7.8 (1.0)	61 (2)	7.8	1
CdA2, X = cdA	dA	Mg^{2+}	260 (30)	0.83 (0.04)	3.2×10^{-3}	4.1×10^{-4}
CdA2. X = A	dA	Mn^{2+}	0.6 (0.1)	46 (1)	77	1
CdA2, X = cdA	dA	Mn^{2+}	0.54 (0.02)	1.10 (0.04)	2.0	2.6×10^{-2}

we eventually obtained cocrystals of Pol η inserting dTTP opposite cdA and extending primers with cdA in the DNA duplex 1 or 2 bp upstream (−1 or −2) from the primer 3′ end. These crystals belonged to two different space groups, $P6_1$ or $P2_12_12_1$, and all contained Pol η, DNA, and an incoming dNTP, which formed a Watson–Crick pair with template base. The resolutions of X-ray diffraction varied from 1.75 to 3.4 Å (*SI Appendix*, Table S1). To better understand the DNA distortion and cytotoxic effects of cdA, we choose to present the highest-resolution structure of cdA first, which is the extension complex with cdA at the −2 position (cdA2; *SI Appendix*, Fig. S1*A* and *B*).

In the cdA2 structure, the *S*-cdA lesion itself is the same as the 0.8-Å crystal structure of the 5′*S*-8,5′-cycloadenosine (25) and nearly superimposable with the NMR structure of *S*-cdG in a short DNA duplex [Protein Data Bank (PDB) ID code 2LFX; *SI Appendix*, Fig. S1*C*] (15). As reported previously (15, 25), the O4′ of cdA is in the exo conformation and points away from the cyclized adenine base. However, the structure of the cdA-containing DNA complexed with DNA Pol η differs from the structures of the free DNA in solution (Fig. 2 *A* and *B*).

The cdA2 structure highlights the backbone and base pair distortions caused by the lesion compared with normal DNA in the complex with Pol η (PDB ID code 4J9O) (26), where a normal dA is in the same position as cdA. Although the overall structural difference is less than 0.6 Å, the largest structural deviations occur at the lesion itself and its base-pairing partner, dT, on the primer strand (Fig. 2 *A, C*, and *D*). The lesion nucleotide cdA is pinched by the C8-C5′ covalent bond, resulting in a 2-Å shift of the deoxyribose toward the minor groove and a closer approach between the phosphate and the adenine base. The phosphate moiety of cdA moves 1.3 Å toward the base, and the cyclized adenine is rotated by ∼30° toward the phosphosugar backbone. As a result, the width of the duplex (e.g., C1′ to C1′) is narrowed by ∼1 Å. In addition, the adenine of cdA is tilted by ∼17° toward the 3′ direction, which leads the base pair 3′ to the cdA [dC (−3)] to buckle and tilt as well (Fig. 2*C*). The cdA loses base stacking with the 5′-neighboring base, which has to overtwist and shift into the major groove to avoid close contact with the O4′ of cdA. The cdA also has lost all hydrogen bonds with its base-pairing partner dT. The orphaned thymine assumes a large roll angle and is displaced into the major groove without base stacking on the 5′ or 3′ side (Fig. 2*C*). Interestingly, the DNA surrounding the abnormal cdA/dT appears little perturbed (Fig. 2*D* and *SI Appendix*, Fig. S1 *D* and *E*), which is probably because of the strength of the flanking C/G pairs and the extensive protein–DNA backbone interactions conferred by the "molecular splint" effect of DNA Pol η (27).

Compared with the crystal structure of DNA-cdA2 complexed with Pol η, the NMR structure of free DNA with an *S*-cdG does not show the dramatically pinched backbone at the lesion or reduced duplex width at the lesion (Fig. 2 *B* and *D*). Instead, cdG remains base paired with dC, and the local distortion is alleviated by a distributive increase of DNA curvature and narrowing of the major groove by ∼3 Å surrounding the lesion.

In the cdA2 structure, the dG at the 3′ end of the primer, with the backbone adjustment, forms a perfect Watson–Crick base pair with the template-strand dC (Fig. 2*C*). Opposite the templating dT, an incoming dATP analog, nonhydrolyzable dAMPNPP (2′-deoxyadenosine-5′-[(α,β)-imido]triphosphate), is coordinated by two Mg^{2+} ions in the active site and is ready for the incorporation reaction as if the cdA lesion did not exist.

Primer Extension Immediately After the cdA Lesion. The crystal structure of Pol η extending a DNA primer immediately after the cdA lesion (cdA1; *SI Appendix*, Table S1) was obtained in the space group of $P2_12_12_1$, which is different from cdA2 and most of the Pol η ternary complexes ($P6_1$) (26–29). Previously, the TLS ternary complex of Pol η bypassing a CPD dimer (PDB ID code 3SI8; henceforth "3SI8") was crystallized in the same space group as cdA1 and appears productive for primer extension (27). In 3SI8, the incoming dATP (dAMPNPP) forms a base pair with the 5′ thymine of the CPD (thymine dimer), and the DNA

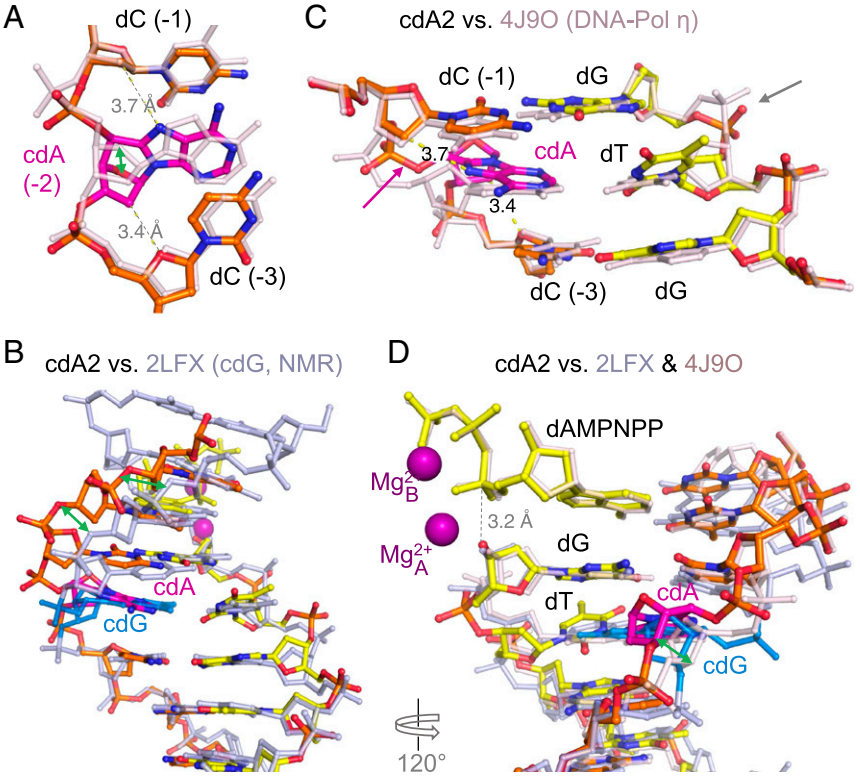

Fig. 2. The cdA2 structure with Pol η engaged in primer extension. (*A*) The structure of cdA and two surrounding bases in cdA2. The corresponding normal DNA in complex with Pol η (PDB ID code 4J9O) is shown as semitransparent pink for comparison. (*B*) Comparison of the crystal structure of cdA-DNA (cdA2; multicolored) and the solution structure of cdG-DNA (PDB ID code 2LFX; blue). The two structures are superimposed at the lesions. DNA duplex upstream of the lesion (lower half) is aligned within 1 Å, whereas downstream DNA (upper half) is more than 2.9 Å apart. (*C*) Close-up view of the three base pairs in cdA2 superimposed with the undamaged DNA bound to Pol η (PDB ID code 4J9O). The distortions of cdA, the displacement of its partner dT, and adjustment of the neighboring dG to form a normal base pair are indicated with arrows. (*D*) Structure superposition of the cdA2 DNA (multicolored) with the DNA without any adduct (PDB ID code 4J9O; pink) and cdG-DNA free in solution (light blue). Large structural changes caused by cdA in complex with Pol η are marked by green double arrowheads in *A*, *B*, and *D*.

substrate and the protein domains are superimposable with active Pol η ternary complexes crystallized in the $P6_1$ space group except for a slightly lifted finger domain (*SI Appendix*, Fig. S2*A*).

The cdA1 structure is significantly different from the Pol η ternary complex structures. Even compared with the CPD structure (3SI8), after superposition of the palm domain and the active site of Pol η, the DNA and the remaining three protein domains of cdA1 all have shifted (Fig. 3*A*). The DNA upstream from the cdA is rotated by ∼20° in the counterclockwise (unwinding) direction, and the associated thumb and little finger (LF) domains are consequently rotated to maintain the DNA interactions. The shift of the LF domain (2.5 Å) is larger than the thumb domain (1.5 Å) because the LF is attached to the palm-thumb domain by a flexible linker. The finger domain in the cdA1 structure is also more open than the CPD bypassing complex.

In the cdA1 structure, although an incoming nucleotide (dAMPNPP) is bound in the active site and coordinated by two Mn^{2+} ions (Fig. 3*A*), Pol η is not engaged in DNA synthesis because the 3′-OH of the DNA primer strand is displaced by >5 Å from the position for in-line attack of the α-phosphate of dAMPNPP (Fig. 3*B* and *SI Appendix*, Fig. S2*B*). The location where the 3′-OH should be is occupied by the phosphate group, which coordinates the A-site Mn^{2+} and renders the active site apparently almost normal. The lesion cdA, which should form a base pair with the dT at the primer 3′ end, is displaced into the major groove and tilted by ∼25°, thus making only van der Waals interactions with the dT at the primer end. The O4′ of cdA perturbs its 5′-neighboring dT and prevents it from assuming the position to base pair with the incoming dATP. As a result, the templating dT is disordered in the cdA1 structure (*SI Appendix*, Fig. S2*C*).

Although the cdA and its 3′-neighboring nucleotide are nearly superimposable between the cdA1 and cdA2 structures, the dT opposite cdA in the cdA2 structure is not in the right position for primer extension (Fig. 3*C*). The observed primer end in the cdA1 structure is somewhat between the correct position as observed in 3SI8 (CPD bypassing complex) and that of dT in the cdA2 duplex. Interestingly, the upstream duplex in cdA2 undergoes even more counterclockwise rotation than that in cdA1 (*SI Appendix*, Fig. S2*D*). Pol η appears to "help" the cdA-containing duplex to adopt the DNA structure suitable for the synthesis reaction, but fails to be fully successful as revealed in the cdA1 structure. The lack of base pairs at the primer end and between the templating base and incoming dNTP explains the error-prone and low-efficiency nature of nucleotide incorporation by Pol η when extending a DNA primer immediately after a cdA lesion (Table 1) (10, 12).

dTTP Incorporation Opposite cdA. To characterize how Pol η incorporates dTTP opposite cdA, we obtained three ternary complex structures in the presence of Mn^{2+}, Mg^{2+}, or Ca^{2+} (*SI Appendix*, Table S1). With the relaxed coordination requirement of Mn^{2+}, the ternary complex structure of Pol η-(cdA)DNA-dTMPNPP (cdA0_Mn; 2′-deoxythymidine-5′-[(α,β)-imido]-triphosphate is a nonhydrolyzable dTTP analog) resembles the structures of a normal purine in the templating position (PDB ID code 4DL2 or 4O3N) (28, 30) (*SI Appendix*, Fig. S3*A*). The active site is completed with the incoming dTMPNPP and two Mn^{2+} ions (Fig. 4*A*). The cdA in the templating position has a similar structure and distortion to that in the duplex of cdA1 and cdA2 complexes (*SI Appendix*, Fig. S3*B*), although the pinched backbone is accommodated in the snug active site and the base tilting is not as severe. The majority of adenine is shifted into the major groove compared with the undamaged templating base, and only ∼40% of adenine takes the same position as a normal template base and is hydrogen bonded with the incoming dTMPNPP (Fig. 4 *B* and *C*). The selection of dTMPNPP for the portion that is not paired with the shifted adenine template may be influenced by the shape complementation and stabilized by the positively charged R61 side chain in the major groove. The 3′-neighboring dC of the cdA is unperturbed and maintains three hydrogen bonds with its partner (dG) at the primer end. The enlarged active site of Pol η, which has evolved to accommodate a CPD dimer, accommodates the cdA lesion. Even its 5′ neighbor (dT, +1) is accommodated in one of two alternative conformations, stacked in or flipped out, similar to the cases of normal DNA substrate (28) (*SI Appendix*, Fig. S3*A*). In solution, dGTP is also incorporated opposite cdA (Fig. 1*B* and Table 1), and guanine may form a Hoogsteen pair with cdA and be stabilized by the interaction of its O6 with R61 in the major groove (26).

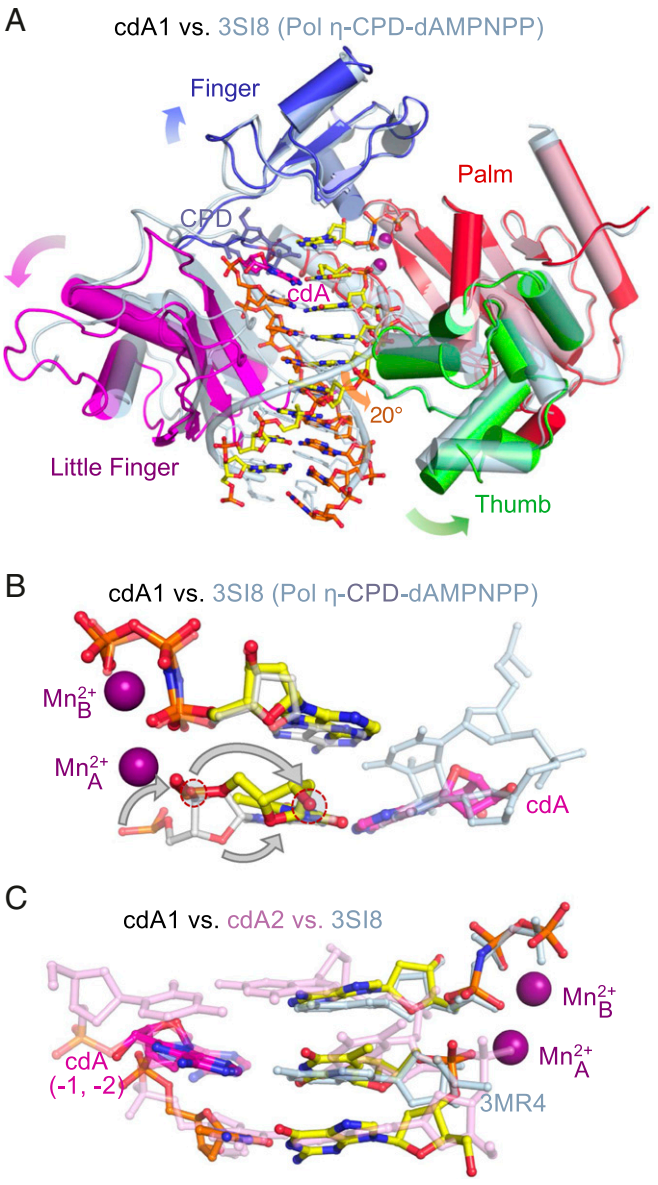

Fig. 3. cdA1 structure. (*A*) cdA1 (multicolored) is superimposed with the structure of CPD bypass by Pol η (PDB ID code 3SI8; blue). Protein domain and DNA movements in cdA1 are indicated by the colored arrowheads. The cdA is severely tilted, and the upstream DNA undergoes a ∼20° counterclockwise rotation (i.e., unwinding). (*B*) Zoom-in view of the two base pairs in the active site. The template base is disordered in cdA1, and the large displacements of the primer 3′ end [deoxyribose, 3′-OH (circled), and phosphate] are indicated by the curved gray arrows. (*C*) Comparison of the DNA structures in cdA1 (multicolored) and cdA2 (pink) after superposition of the cdA. The productive conformations of the primer 3′ end and the incoming nucleotide positions are represented by the 3SI8 structure (blue) after superimposing Pol η.

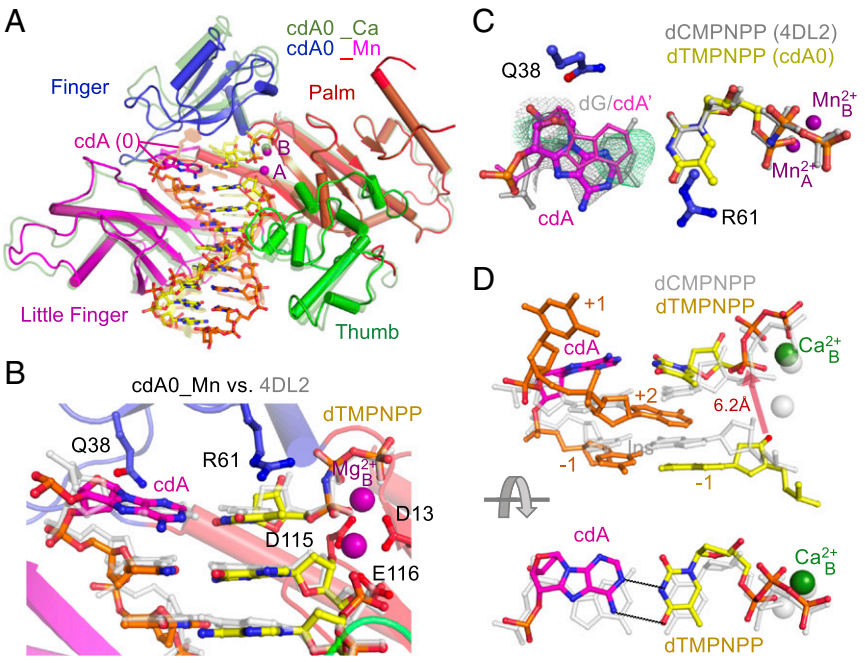

Fig. 4. Structures of nucleotide incorporation opposite cdA. (*A*) Structure superposition of cdA0 in the presence of Mn^{2+} (multicolored) and Ca^{2+} (semitransparent green Pol η and yellow/orange DNA duplex shown as cartoon tubes). (*B*) Close-up view of the active site of cdA0_Mn superimposed with a lesion-free DNA in complex with Pol η (PDB ID code 4DL2; gray). (*C*) The replicating base pair in cdA0_Mn resembles that in 4DL2 structure except that the majority of cdA base (cdA) is shifted into the major groove. The minority of cdA adopts the normal templating position (cdA′) as shown by the thinner stick and lighter magenta color. The 2Fo-Fc (silver mesh, contoured at 1.0σ) and Fo-Fc omit map (green mesh, contoured at 3σ), which were calculated without the minor conformer of cdA, are superimposed. Protein side chains Q39 and R61 appear to stabilize the lesion pair. (*D*) Two orthogonal views of the base pairs in the cdA0_Ca structure. The corresponding base pairs from the normal Pol η complex (PDB ID code 4DL2) are shown in semitransparent gray for comparison.

In contrast to the nearly normal active-site configuration with Mn^{2+}, in the presence of Mg^{2+} or Ca^{2+}, the constraints imposed by the cdA led to a gross rearrangement of the template strand and opening of the finger domain to accommodate the DNA change (Fig. 4*A*). Because Ca^{2+} does not support the DNA synthesis reaction, dTTP was used in cocrystallization. Interestingly, the structures of Pol η complexed with Mg^{2+}/dTMPNPP (cdA0_Mg) or Ca^{2+}/dTTP (cdA0_Ca) are superimposable (*SI Appendix*, Fig. S3*C*). When complexed with Mg^{2+} or Ca^{2+}, the downstream ssDNA template makes a U-turn with the +1 nucleotide (dT) 5′ of cdA bent 120° toward the major groove and the +2 nucleobase (dA) intercalated between the replicating base pair (0) and the base pair at the primer end (−1; Fig. 4*D*). Consequently, the 3′-OH of the primer is >6 Å instead of the normal 3.2 Å away from the α-phosphate of the incoming nucleotide. Only the B-site metal ion remains associated with the triphosphate of an incoming nucleotide, and the A-site is empty.

With Ca^{2+}, the templating cdA forms a severely buckled base pair with dTTP; however, with Mg^{2+}, only one hydrogen bond is maintained between the cdA and dTMPNPP as the cdA shifts toward the minor groove and thymine base is shifted toward the major groove (*SI Appendix*, Fig. S3*D*). Overall, the structure in the presence of Mg^{2+} is less ordered and less "engaged" than that of Ca^{2+}. The cdA0_Mg structure likely gives way to a much less populated yet productive complex like the one with Mn^{2+} bound for dNTP incorporation as observed in solution (Fig. 1*B*).

Discussion

Environmental Effects on DNA Structures and TLS of cdA. Cyclization between a 2′-deoxyribose and purine base makes cdPu rather rigid, and the structural details of cdPu are conserved regardless of the base being guanine or adenine and whether in solution or crystal. However, the global DNA structure in the presence of a cdPu is influenced by the environment and differs between protein-free and protein-bound states (Fig. 2 *B* and *D*). The cdA-DNA also changes structures in cdA0, cdA1, and cdA2 complexes as the DNA experiences different parts of the molecular splint of Pol η (*SI Appendix*, Fig. S2*D*). The covalent bond between C5′ of the deoxyribose and C8 of purine leads to a pinched phosphosugar backbone toward the minor groove and close contacts of the O4′ and C2′ of the cdPu with the 5′ and 3′ neighboring nucleotides, respectively. When free from protein, close contacts are avoided by the 5′ neighbor, which assumes a large twist angle and shifts toward the major groove, resulting in an increased DNA curvature and narrowed major groove (Fig. 2*B*). When complexed with DNA Pol, the molecular splint of Pol η, which forms complementary interactions with five consecutive phosphates of the upstream template strand, has a strong influence on the local distortions surrounding the cdA and overall DNA structures. Pol η is able to accommodate the cdA at the −2 position for primer extension, but is unable to stabilize the templating base to pair with an incoming nucleotide when the cdA is at the −1 position.

Interestingly, DNA distortions induced by cdA, including base tilting and shifting toward the major groove and over-twisting of the 5′ neighbor, resemble the DNA substrate conformation in complex with another Y-family member, Pol ι (12). In addition, the pinched backbone of cdA narrows the duplex width and makes it a match for Pol ι, which has a narrow space for the nascent base pair and thus reportedly prefers a Hoogsteen pair over the normal Watson–Crick pair (31, 32). Pol ι has been shown to be able to incorporate dTTP or dGTP opposite *S*-cdA with similar efficiency as Pol η (12).

Effects of Divalent Cations on TLS. As has long been established, Mn^{2+} relaxes the substrate selection and supports dNTP incorporation in the presence of a noncognate Watson–Crick base pair (33). The effect of Mn^{2+} in dNTP binding by Pol η in the presence of *S*-cdA is dramatic. Mn^{2+} increases the dNTP binding by 100–2,000 fold with the lesion-containing DNA, but changes K_M of dNTP by only 1–10 fold on undamaged DNAs (Table 1). The cdA0_Mn structure illustrates the effect of Mn^{2+} on enabling dTMPNPP to bind in the same conformation as the incorporation reaction, even though the templating cdA is not base-paired with dTMPNPP. It has been suspected that Mg^{2+} increases the fidelity of DNA Pols by "amplifying" the small energy differences of a mismatched base pair to make orders of magnitude differences in catalytic efficiencies (33, 34). When DNA and dNTP are normal and base-paired, the catalytic efficiencies of DNA synthesis in the presence of Mg^{2+} or Mn^{2+} are rather similar. The dramatic structural differences between cdA0_Mn and cdA0_Mg demonstrate just how big a difference these divalent cations make when a

DNA Pol is challenged by noncognate substrate and absence of Watson–Crick base pairs. It has been difficult to compute the free energy contributed by metal ion ligands, but the contrasting cdA0 structures and 1,000-fold different catalytic efficiencies indicate these metal-ion ligands contribute much more than the equivalence of a couple of hydrogen bonds.

Cytotoxicity and Mutagenicity of cdPu. As shown in the NMR and crystallographic structures, the *S*-diastereomers of cdA and cdG are compatible with the normal B-form DNA with moderate local distortions to the DNA duplex. However, the corresponding *R*-diastereomers could not be accommodated in DNA without significant disruption. The relatively mild distortions of DNA duplex by *S*-cdPus make detection of these lesions for repair difficult unless detected by stalled transcription machineries, which may explain the lesion accumulation in the aging process.

The cdPus are strong roadblocks to cellular DNA replication machinery, and the replication bypass efficiencies of *S*-cdA and *S*-cdG in HEK293T cells are ∼6% and 4% relative to unmodified dA and dG, respectively (12). In addition, *S*-cdA induces T→A transversion at a frequency of ∼12% in HEK293T cells (12). Our analyses provide structural insights into the replication blockage by cdA and substantiate the role of Pol η in promoting bypass of *S*-cdA. The cdA0 structures, however, indicate that, in the presence of physiologically relevant Mg^{2+}, Pol η is often engaged in a nonproductive conformation with cdA in the templating position and likely has low TLS activity. When Pol η fails, other Pols may follow the "A" rule, which ultimately gives rise to T→A mutation. Although these cdPus allow limited replication bypass, their moderate mutagenic effect (12) agrees well with the finding that patients with xeroderma pigmentosum, who are incapable of repairing cdPu lesions, have relatively low incidences of internal cancers (14).

Methods

Synthesis and Preparation of Oligodeoxyribonucleotides Containing 5′*S*-cdA Lesions. Oligodeoxyribonucleotides containing a site-specifically incorporated 5′*S*-cdA for TLS assays and cocrystallization with human DNA Pol η were synthesized following previously published procedures (35) and summarized in Fig. 1.

Preparation of Human DNA Pol η and Crystallization. Human core DNA Pol η was expressed and purified as described previously (27).

Structure Determination. Statistics of data collection and structure refinement are summarized in *SI Appendix*, Table S1.

Assays of Nucleotide Selection and Efficiency in TLS. Incorporation opposite cdA and primer extensions were assayed according to the published procedure (28).

ACKNOWLEDGMENTS. We thank R. Craigie and D. Leahy for critical reading of the manuscript. This research was supported by National Institutes of Health (NIH) Intramural Funding DK036146 (to W.Y.) and NIH Grant R01 CA210072 (to Y.W.).

1. Jaruga P, Dizdaroglu M (2008) 8,5′-cyclopurine-2′-deoxynucleosides in DNA: Mechanisms of formation, measurement, repair and biological effects. *DNA Repair (Amst)* 7: 1413–1425.
2. Whitaker AM, Schaich MA, Smith MR, Flynn TS, Freudenthal BD (2017) Base excision repair of oxidative DNA damage: From mechanism to disease. *Front Biosci* 22: 1493–1522.
3. Brooks PJ, et al. (2000) The oxidative DNA lesion 8,5′-(S)-cyclo-2′-deoxyadenosine is repaired by the nucleotide excision repair pathway and blocks gene expression in mammalian cells. *J Biol Chem* 275:22355–22362.
4. Kuraoka I, et al. (2000) Removal of oxygen free-radical-induced 5′,8-purine cyclodeoxynucleosides from DNA by the nucleotide excision-repair pathway in human cells. *Proc Natl Acad Sci USA* 97:3832–3837.
5. Theruvathu JA, Jaruga P, Dizdaroglu M, Brooks PJ (2007) The oxidatively induced DNA lesions 8,5′-cyclo-2′-deoxyadenosine and 8-hydroxy-2′-deoxyadenosine are strongly resistant to acid-induced hydrolysis of the glycosidic bond. *Mech Ageing Dev* 128: 494–502.
6. Kropachev K, et al. (2014) Structural basis for the recognition of diastereomeric 5′,8-cyclo-2′-deoxypurine lesions by the human nucleotide excision repair system. *Nucleic Acids Res* 42:5020–5032.
7. Yang W (2011) Surviving the sun: Repair and bypass of DNA UV lesions. *Protein Sci* 20: 1781–1789.
8. Wang J, Clauson CL, Robbins PD, Niedernhofer LJ, Wang Y (2012) The oxidative DNA lesions 8,5′-cyclopurines accumulate with aging in a tissue-specific manner. *Aging Cell* 11:714–716.
9. Iwamoto T, et al. (2014) Quantitative and in situ detection of oxidatively generated DNA damage 8,5′-cyclo-2′-deoxyadenosine using an immunoassay with a novel monoclonal antibody. *Photochem Photobiol* 90:829–836.
10. Kuraoka I, et al. (2001) Oxygen free radical damage to DNA. Translesion synthesis by human DNA polymerase eta and resistance to exonuclease action at cyclopurine deoxynucleoside residues. *J Biol Chem* 276:49283–49288.
11. Walmacq C, et al. (2015) Mechanism of RNA polymerase II bypass of oxidative cyclopurine DNA lesions. *Proc Natl Acad Sci USA* 112:E410–E419.
12. You C, et al. (2013) Translesion synthesis of 8,5′-cyclopurine-2′-deoxynucleosides by DNA polymerases η, ι, and ζ. *J Biol Chem* 288:28548–28556.
13. Jaruga P, Theruvathu J, Dizdaroglu M, Brooks PJ (2004) Complete release of (5′S)-8,5′-cyclo-2′-deoxyadenosine from dinucleotides, oligodeoxynucleotides and DNA, and direct comparison of its levels in cellular DNA with other oxidatively induced DNA lesions. *Nucleic Acids Res* 32:e87.
14. Brooks PJ (2017) The cyclopurine deoxynucleosides: DNA repair, biological effects, mechanistic insights, and unanswered questions. *Free Radic Biol Med* 107:90–100.
15. Huang H, Das RS, Basu AK, Stone MP (2011) Structure of (5′S)-8,5′-cyclo-2′-deoxyguanosine in DNA. *J Am Chem Soc* 133:20357–20368.
16. Huang H, Das RS, Basu AK, Stone MP (2012) Structures of (5′S)-8,5′-Cyclo-2′-deoxyguanosine mismatched with dA or dT. *Chem Res Toxicol* 25:478–490.
17. Xu W, et al. (2015) Kinetic and structural mechanisms of (5′S)-8,5′-cyclo-2′-deoxyguanosine-induced dna replication stalling. *Biochemistry* 54:639–651.
18. Swanson AL, Wang J, Wang Y (2012) Accurate and efficient bypass of 8,5′-cyclopurine-2′-deoxynucleosides by human and yeast DNA polymerase η. *Chem Res Toxicol* 25:1682–1691.
19. Shachar S, et al. (2009) Two-polymerase mechanisms dictate error-free and error-prone translesion DNA synthesis in mammals. *EMBO J* 28:383–393.
20. Lee YS, Gregory MT, Yang W (2014) Human Pol ζ purified with accessory subunits is active in translesion DNA synthesis and complements Pol η in cisplatin bypass. *Proc Natl Acad Sci USA* 111:2954–2959.
21. Yang W (2014) An overview of Y-Family DNA polymerases and a case study of human DNA polymerase η. *Biochemistry* 53:2793–2803.
22. Yang W (2006) Poor base stacking at DNA lesions may initiate recognition by many repair proteins. *DNA Repair (Amst)* 5:654–666.
23. Wang F, Yang W (2009) Structural insight into translesion synthesis by DNA Pol II. *Cell* 139:1279–1289.
24. Lee YS, Gao Y, Yang W (2015) How a homolog of high-fidelity replicases conducts mutagenic DNA synthesis. *Nat Struct Mol Biol* 22:298–303.
25. Haromy TP, Raleigh J, Sundaralingam M (1980) Enzyme-bound conformations of nucleotide substrates. X-ray structure and absolute configuration of 8,5′-cyclo-adenosine monohydrate. *Biochemistry* 19:1718–1722.
26. Zhao Y, et al. (2013) Mechanism of somatic hypermutation at the WA motif by human DNA polymerase η. *Proc Natl Acad Sci USA* 110:8146–8151.
27. Biertümpfel C, et al. (2010) Structure and mechanism of human DNA polymerase eta. *Nature* 465:1044–1048.
28. Zhao Y, et al. (2012) Structural basis of human DNA polymerase η-mediated chemoresistance to cisplatin. *Proc Natl Acad Sci USA* 109:7269–7274.
29. Gregory MT, et al. (2014) Structural and mechanistic studies of polymerase η bypass of phenanthriplatin DNA damage. *Proc Natl Acad Sci USA* 111:9133–9138.
30. Patra A, et al. (2014) Kinetics, structure, and mechanism of 8-Oxo-7,8-dihydro-2′-deoxyguanosine bypass by human DNA polymerase η. *J Biol Chem* 289:16867–16882.
31. Nair DT, Johnson RE, Prakash L, Prakash S, Aggarwal AK (2006) Hoogsteen base pair formation promotes synthesis opposite the 1,N6-ethenodeoxyadenosine lesion by human DNA polymerase iota. *Nat Struct Mol Biol* 13:619–625.
32. Kirouac KN, Ling H (2009) Structural basis of error-prone replication and stalling at a thymine base by human DNA polymerase iota. *EMBO J* 28:1644–1654.
33. Yang W, Woodgate R (2007) What a difference a decade makes: Insights into translesion DNA synthesis. *Proc Natl Acad Sci USA* 104:15591–15598.
34. Gao Y, Yang W (2016) Capture of a third Mg^{2+} is essential for catalyzing DNA synthesis. *Science* 352:1334–1337.
35. Yuan B, Wang J, Cao H, Sun R, Wang Y (2011) High-throughput analysis of the mutagenic and cytotoxic properties of DNA lesions by next-generation sequencing. *Nucleic Acids Res* 39:5945–5954.